On the Statistical Nature of Collision and Surface-Induced Dissociation: A Theoretical Investigation of Aluminum Clusters[†]

Pascal Larrégaray[§] and Gilles H. Peslherbe*

Centre for Research in Molecular Modeling and Department of Chemistry & Biochemistry, Concordia University, Montreal, QC Canada H4B 1R6

The unimolecular dissociation dynamics of aluminum clusters following collision with either a rare gas atom or a surface is investigated by classical trajectory simulations with model potentials. Two conformers of Al_6 with very distinct shapes, i.e., the spherical O_h and planar C_{2h} clusters, are considered in this work. The initial vibrational energy and angular momentum distributions resulting from collision, as well as the energy and angular momentum resolved lifetime distributions, of excited clusters were determined for both collision-induced dissociation (CID) and surface-induced dissociation (SID) processes. The partitioning of excitation energy acquired upon collision was found to depend on the excitation mechanism (CID or SID), as well as on the cluster molecular shape, especially in the case of CID. For both types of processes, the energy and angular momentum resolved excited cluster lifetime distributions were found to decay exponentially, in agreement with statistical theories of chemical reactions, suggesting intrinsic Rice−Ramsperger−Kassel−Marcus (RRKM) behavior. Moreover, the simulated microcanonical rate constants determined from the cluster lifetime distributions are in good agreement with the predictions of the orbiting transition state model of phase space theory (OTS/PST), which further supports the statistical character of cluster CID and SID. Thus, in the CID and SID of highly fluxional systems such as aluminum clusters, the rate of intramolecular vibrational energy redistribution (IVR) is much faster than the dissociation rate, which validates one of the key assumptions, i.e., post-collision statistical behavior, underlying the models that are routinely used to determine cluster binding energies from experimental CID/SID cross sections.

I. Introduction

Clusters have been the focus of a tremendous number of theoretical and experimental studies.[1−3] On one hand, weakly bound atomic or molecular clusters can be viewed as "finite-size pieces of condensed matter",[4] and investigating their properties may help gain insight into microsolvation effects. On the other hand, more strongly bound atomic clusters, such as semiconductors or metallic ones, exhibit a wide range of size and shape-dependent chemical properties,[5,6] which motivates in part the huge current interest in nanotechnologies. Moreover, these clusters have been employed as models for surfaces, for instance to investigate heterogeneous catalysis. More generally, cluster studies may help understand how chemical properties evolve from the gas to the condensed phases.[1−4] Of particular interest is the dissociation of cluster materials induced by collisions with surfaces or rare gas atoms, as they provide insight into the stability of such species.

The dynamics of cluster dissociation is expected to exhibit very different patterns, depending on the nature of the interactions between the atoms or molecules constituting the cluster. When a chemical species is vibrationally excited, if the coupling between the internal degrees of freedom is strong enough, energy flows freely between the various vibrational modes and is thus redistributed statistically among these modes. Statistical theories of chemical reactions,[7−14] which assume that the average time for this intramolecular vibrational energy redistribution (IVR) is much shorter than the average time for dissociation, then turn out to be extremely powerful in predicting and rationalizing kinetics and dynamical observables such as rate constants and product energy distributions. For instance, IVR is usually fast in molecules constituted of atoms linked by covalent bonds, even though a few examples of nonstatistical behavior have been reported in the literature.[14−18] In contrast, if the coupling between the various modes of a chemical species is very weak, IVR may not take place before dissociation, the dynamics is nonstatistical and strongly dependent on the excitation process. This behavior has been evidenced experimentally for some weakly bound dimers containing one chromophore molecule.[14] The chromophore can be vibrationally excited by photon absorption over the dimer dissociation threshold, and energy transfer to the intermolecular van der Waals modes upon chromophore vibrational relaxation promotes dimer dissociation. Rate constants for such phenomenon, known as vibrational predissociation,[19−21] are highly dependent on the chromophore initial excited vibrational state. For molecular or atomic clusters, given the wide range of interactions that exist, depending on the nature of the cluster constituents and the total charge,[14] an a priori prediction of the dynamical behavior is not straightforward.

Besides being of fundamental interest, characterizing cluster dissociation dynamics is also of practical interest, because cluster structural properties, such as binding energies, are often inferred from experimental data with the use of statistical models. In

Statistical Nature of Collision and Surface-Induced Dissociation

J. Phys. Chem. A, Vol. 110, No. 4, 2006 **1659**

typical collision-induced and surface-induced dissociation experiments (CID and SID, respectively), the cluster dissociation cross section is measured as a function of the collision energy and fitted to an empirical law.[6,22] However, the finite-lifetime observation window may be comparable to the time scale for cluster dissociation and responsible for a "kinetic shift" of the observed threshold. For instance, in this case, the energy-dependent expression for the CID cross section must be corrected for the cluster finite lifetime,[23-25] which is usually estimated by statistical theories such as phase space theory (PST) or Rice–Ramsperger–Kassel–Marcus (RRKM) theory.[14] Similarly, experimental cluster photodissociation lifetime distributions can be fit to a statistical rate theory expression to extract the cluster binding energy as the activation energy for dissociation.[26,27] Another experimental approach consists of analyzing the product translational energies, which can be related to the cluster binding energy with the help of approximate statistical models.[28-32] In all experiments, clusters are assumed to dissociate statistically. Thus, it appears necessary to test this assumption, which motivates the present work on aluminum clusters.

In the last two decades, charged or neutral aluminum clusters have been the subject of a large number of experimental[26,33-47] and theoretical[48-54] studies, aiming mainly at determining their structural properties and fragmentation pathways. Theoretical investigations of their dissociation dynamics[55-57] and of energy transfer in CID processes[58] have recently been reported. For instance, ensembles of Al_6 and Al_{13}, sampled from an approximate microcanonical distribution, i.e., with energy randomly distributed over all cluster vibrational modes, were shown to dissociate statistically.[55,59] Furthermore, the energy (E) and total angular momentum (J) resolved anharmonic dissociation rate constants,[55] as well as the product energy partitioning,[59] predicted within the framework of the orbiting transition state/phase space theory (OTS/PST)[60-63] were found to be in very good agreement with the results of classical trajectory simulations. These findings suggest that the dissociation of Al_n clusters is intrinsically RRKM, and that there is no bottleneck to energy transfer between vibrational modes. On the other hand, the initial energy distribution in clusters excited by collisions with surfaces or rare gas atoms may be far from being microcanonical. The goal of this work is to investigate the unimolecular dissociation of clusters excited by collision and characterize IVR. To investigate the possible dependence of IVR on the excitation mechanism, we simulated the dissociation of Al_6 clusters excited by both collisions with an argon (Ar) atom and with a rigid surface. Classical trajectory simulations were performed and the energy and total angular momentum resolved distributions of excited cluster lifetimes were determined, leading to simulated microcanonical dissociation rate constants. These results were then compared to those obtained with an accurate statistical theory.

The outline of this article is as follows. The simulation procedure and statistical theory expressions are briefly reviewed in section II. The results of simulations and statistical rate theories are then presented and discussed in section III. Conclusions follow in section IV.

II. Computational Procedure and Theory

A. Classical Trajectory Simulations. Classical trajectory simulations of Al_6 collision- and surface-induced dissociation were performed with the general chemical dynamics computer program VENUS.[64] The Al_n potential energy function and the simulation methodology are the same as in previous work,[55-59] and are only briefly reviewed here for completeness.

The Al_n potential function, fitted to ab initio electronic structure calculations,[54] is a sum of two body Lennard-Jones (L-J) potentials

$$V_{ij} = \frac{A}{r_{ij}^{12}} + \frac{B}{r_{ij}^{6}} \quad (1)$$

and three-body Axilrod–Teller (A–T) potentials[65]

$$V_{ijk} = C\frac{1 + 3\cos\alpha_{ijk}\cos\alpha_{jki}\cos\alpha_{kij}}{(r_{ij}r_{jk}r_{ki})^3} \quad (2)$$

with parameters $A = 2\,975\,343.77$ kcal Å^{12} mol^{-1}, $B = -17\,765.823$ kcal Å^6 mol^{-1}, and $C = 81\,286.093$ kcal mol^{-1}. In eq 2 r_{ij}, r_{jk}, r_{ki}, and α_{ijk}, α_{jki}, α_{kij} are the sides and angles, respectively, of the triangle formed by three atoms i, j, and k. The relative merits of this model potential have been discussed elsewhere.[58,59] We note, however, that the model potential predicts energetics and minimum energy structures of small clusters in good agreement with ab initio calculations.[66] As Al_n clusters are very fluxional molecules, i.e., they are characterized by a large number of minimum energy structures of comparable stability, with barriers for isomerization much lower than the dissociation threshold,[55] simulations are performed for two conformers of different compacity (with O_h and C_{2h} symmetry) to infer the influence of cluster shape in CID/SID dynamics. The structural properties and dissociation energies of the O_h and C_{2h} clusters are listed in Table 1.
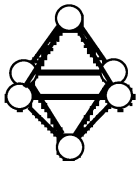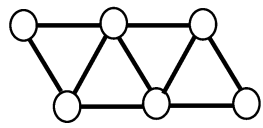
For CID simulations, the interaction potential between the colliding argon (Ar) atom and each Al atom is given by the two-body term

$$V = \frac{a}{r^{12}} + \frac{b}{r^6} + c\,e^{-dr_1} \quad (3)$$

where r is the distance between the Ar and Al atoms. The parameters $a = 5212.132$ kcal Å^{12} mol^{-1}, $b = 884.959$ kcal Å^6 mol^{-1}, $c = 10\,421.443$ kcal mol^{-1}, and $d = 2.753\,02$ Å^{-1} were simply fitted to high level ab initio calculations.[58] For SID simulations, we employ a simple hard surface model, where atomic velocities in the direction normal to the surface are reversed upon impact.[67] Moreover, only normal collisions are considered, i.e., the initial cluster center-of-mass velocity is always set orthogonal to the surface. The influence of the incidence angle will be studied in future work.

In all simulations, the collisional energy is set to 120.8 kcal mol^{-1}, which corresponds to the experimental collision energy of 5.24 eV,[41-43] and clusters are initially randomly oriented with respect to the surface or the colliding atom. For CID, the initial cluster-atom distance is set to 50 Å, and the impact parameter b is randomly selected between 0 and the maximum value b_{max}, which is chosen as 3.5 and 5.5 Å for the O_h and C_{2h} clusters, respectively, on the basis of previous work.[58] For SID, the initial cluster-surface distance is also set to 50 Å. The clusters are given an amount of energy $RT/2$ along each of the principal axes of rotation, with a rotational temperature of 138 K, to be consistent with previous theoretical and experimental studies.[41,43,57] The effect of zero-point energy on the unimolecular dissociation dynamics was previously found to be negligible,[58] so that no vibrational energy is initially added to the cluster, and all vibrational energy is thus acquired upon collision with the surface or the colliding atom. All clusters acquiring a vibrational energy above the dissociation threshold are likely to dissociate, and such trajectories are integrated for 500 ps after collision. Because of the weak rotation–vibration coupling,

TABLE 1: Cluster Structures and Dissociation Thresholds

	O_h		C_{2h}	
$r_e{}^a$ = 2.83 Å			$r_e{}^a$ = 2.72 Å	

dissociation channel	$Al_6 \rightarrow Al_5 + Al$	$Al_6 \rightarrow Al_4 + Al_2$	$Al_6 \rightarrow Al_3 + Al_3$
E_0 (O_h) kcal·mol^{-1}	38.8	55.4	57.8
E_0(C_{2h}) kcal·mol^{-1}	43.8	60.4	63.8

^{a} Average nearest neighbor equilibrium distance. ^{b} Threshold for dissociation on the potential energy surface of eqs 1 and 2.

clusters acquiring a total internal energy greater than the dissociation threshold, but with vibrational energy lower than threshold, are not likely to dissociate within this lapse of time and trajectories corresponding to this situation are thus not propagated any longer. The excited cluster lifetime is estimated as the time between impact with the colliding atom or the surface and the time at the last turning point in the relative motion of the products' center of mass. In SID simulations, multiple collisions generally occur and the impact time, i.e., the time reference for cluster dissociation, is the time of the last collision between any cluster atom and the surface.

B. Statistical Theory. For unimolecular statistical processes, the evolution of the normalized reactant population as a function of time (i.e., lifetime distribution) follows a first-order dissociation rate law, i.e.

$$P_{E,J}(t) = \frac{N_{E,J}(t)}{N_{E,J}(0)} = e^{-k(E,J)t} \tag{4}$$

where $N_{E,J}(0)$ is the initial number of reactant species with total energy E and angular momentum J, $N_{E,J}(t)$ the number of remaining undissociated species at time t, and $k(E,J)$ is the microcanonical unimolecular rate constant.

The microcanonical unimolecular rate constant $k(E,J)$ can be calculated within the framework of transition state theory (TST)[7,14] as

$$k(E,J) = \frac{L^{\ddagger}N^{\ddagger}(E,J)}{h\rho(E,J)} \tag{5}$$

where h is Planck's constant, $N^{\ddagger}(E,J)$ is the sum of states at the transition state, $L^{\ddagger}$ is the reaction channel statistical factor (or degeneracy), and $\rho(E,J)$ is the density of states of the reactant molecule. All existing statistical theories of chemical reactions simply differ in the way these quantities are evaluated.[7,68] For aluminum cluster unimolecular dissociation, orbiting transition state/phase space theory (OTS/PST), which is an improved version of PST[14] in which the transition state is located at the top of the centrifugal barrier along the reaction coordinate[60−63] instead of lying at the product asymptotic limit, was found to predict microcanonical rate constants in good agreement with those obtained from simulations.[55]

Because of the fluxional nature of Al_n clusters, anharmonicity significantly affects the reactant density of states $\rho(E,J)$ and the transition state number of states $N^{\ddagger}(E,J)$.[55] Anharmonic densities

TABLE 2: Dissociation Pathway Partitioning^a

dissociation channel:		$Al_6 \rightarrow Al_5 + Al$	$Al_6 \rightarrow Al_4 + Al_2$	$Al_6 \rightarrow Al_3 + Al_3$
CID	O_h	97.9	1.8	0.3
	C_{2h}	97	2.6	0.4
SID	O_h	91	7	2
	C_{2h}	88	10	2

^{a} % of reactive dissociation occurring within 500 ps.

TABLE 3: Types of Dissociation Events^a

		direct dissociation	dissociation within 500 ps	dissociation after 500 ps
CID	O_h	13	47	40
	C_{2h}	14	46	40
SID	O_h	6	75	19
	C_{2h}	5	74	21

^{a} % of reactive dissociation.

of states for both reactants and products (the latter is required to compute the transition state number of states) have been evaluated in previous work.[55] As stated earlier, OTS/PST microcanonical rate constants and those calculated from CID/SID classical trajectory simulations are expected to agree only if IVR is so fast with respect to the average time for dissociation that the phase space state distribution is approximately microcanonical immediately following excitation, in this case, collision with a surface or rare gas atom.

III. Results and Discussion

The dissociation pathway partitioning (monomer, dimer, and trimer formation) is presented in Table 2 for both CID and SID. In all simulations, the monomer evaporation channel, which is energetically more favorable, is not surprisingly the main dissociation pathway for both O_h and C_{2h} conformers regardless of the mechanism of excitation. Thus, in the following, we mainly focus on this dissociation channel. Furthermore, in both CID and SID processes, a significant fraction of clusters were found to dissociate instantaneously upon collision; i.e., the evaporating atoms are not involved in a single vibrational motion before dissociating (cf. Table 3). These events are called "direct dissociation" in the following.

A. Al_6 Vibrational Energy and Angular Momentum Distributions. The distributions of vibrational energy acquired by the Al_6 cluster upon collision in the CID process are displayed in Figure 1. The vibrational energy distributions are
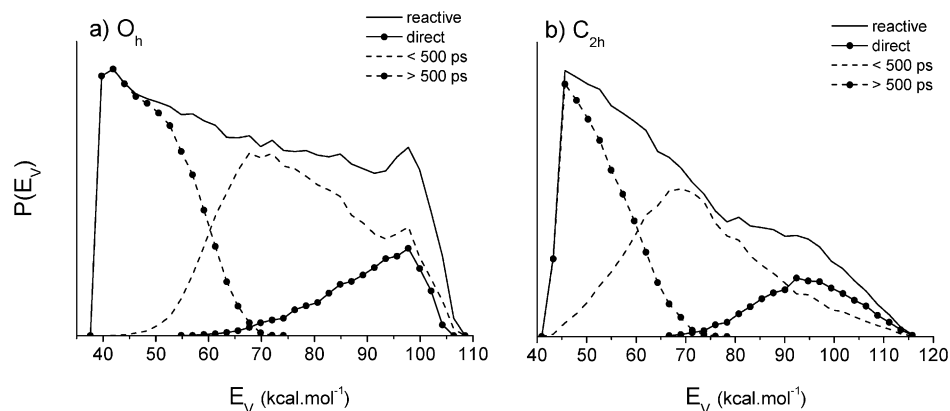
Statistical Nature of Collision and Surface-Induced Dissociation

J. Phys. Chem. A, Vol. 110, No. 4, 2006 **1661**

Figure 1. CID vibrational energy distributions for reactive (a) O_h and (b) C_{2h} Al$_6$ clusters: all reactive clusters (solid line), clusters dissociating within 500 ps (dashed line), clusters dissociating after 500 ps (dotted-dashed line), clusters dissociating directly (dotted solid line). Results are based on 40 000 trajectories dissociating within 500 ps.
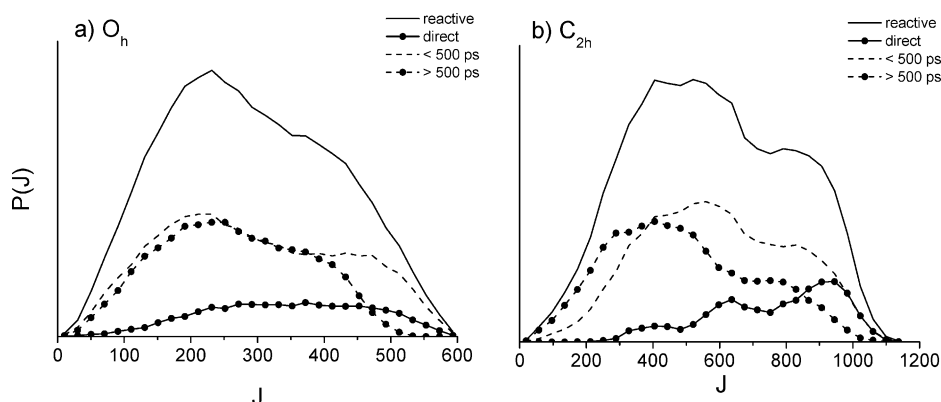

Figure 2. CID angular momentum distributions for reactive (a) O_h and (b) C_{2h} Al$_6$ clusters: all reactive clusters (solid line), clusters dissociating within 500 ps (dashed line), clusters dissociating after 500 ps (dotted-dashed line), clusters dissociating directly (dotted solid line). Results are based on 40 000 trajectories dissociating within 500 ps.

given for all reactive clusters, i.e., for clusters with an initial vibrational energy greater than threshold (solid line), all the excited clusters dissociating within 500 ps (dashed line), all those eventually dissociating after 500 ps, i.e., with an energy greater than threshold but not dissociative on the simulation time scale (dotted dashed line) and those involving "direct" dissociation (solid dotted line). The proportion of each type of event is given in Table 3. The distributions are normalized so that the area under the distribution curve is the same for all reactive events in all plots.

The initial vibrational energy distributions exhibit similar features for both O_h and C_{2h} cluster CID. A large fraction of collisions do not transfer enough energy to the cluster to allow dissociation within 500 ps. This trend is more pronounced in the case of the O_h cluster. For both conformers, a large fraction of clusters with an excess vibrational energy between 20 and 50 kcal mol^{-1} above threshold dissociate within 500 ps. For larger excitation energies, the amount of direct dissociation becomes significant. We note that the fraction of clusters excited with an energy close to threshold is larger in the case of the C_{2h} conformer than in the case of the O_h one. As a result, the average vibrational energies in excess of threshold are about 29 and 24.5 kcal mol^{-1} for the O_h and C_{2h} conformers, respectively. This corresponds to roughly the same average vibrational energy with respect to the Al$_6$ ground-state minimum configuration. Thus, the average energies transferred to vibration upon collision are nearly identical for both clusters, although the distributions of energy are slightly different. For instance, a much smaller fraction of clusters acquire very high vibrational
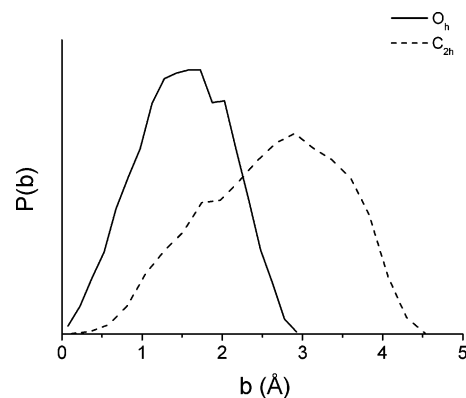

Figure 3. CID opacity functions for direct cluster dissociation of Al$_6$ O_h clusters (solid line) and C_{2h} clusters (dashed line). Results are based on 40 000 trajectories dissociating within 500 ps.

energy (i.e. larger than 70 kcal/mol above threshold) for C_{2h} conformers than for O_h ones.

Figure 2 displays the Al$_6$ cluster total angular momentum distributions following collisional excitation. Rotational excitation is obviously much more significant in the case of the C_{2h} cluster. The average angular momentum quantum numbers are $\approx$290 and $\approx$580 for the O_h and C_{2h} conformers, respectively. These trends are similar to those previously observed[58] and can be intuitively understood on the basis of the shape of the two conformers. The less compact C_{2h} conformer (6.8 Å long vs 4 Å for the O_h one) is naturally expected to involve collisions at larger impact parameters, for which a significant part of the
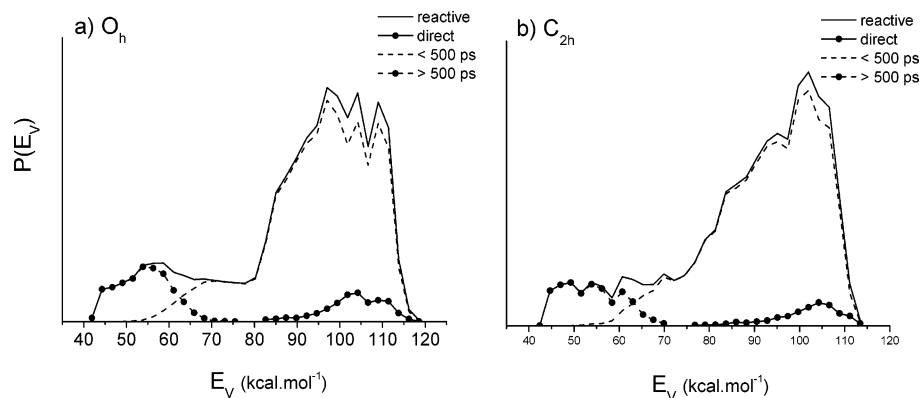
Figure 4. SID vibrational energy distributions for reactive (a) O_h and (b) C_{2h} Al$_6$ clusters: all reactive clusters (solid line), clusters dissociating within 500 ps (dashed line), clusters dissociating after 500 ps (dotted-dashed line), clusters dissociating directly (dotted solid line). Results are based on 40 000 trajectories dissociating within 500 ps.

Figure 5. SID angular momentum distributions for reactive (a) O_h and (b) C_{2h} Al$_6$ clusters: all reactive clusters (solid line), clusters dissociating within 500 ps (dashed line), clusters dissociating after 500 ps (dotted-dashed line), clusters dissociating directly (dotted solid line). Results are based on 40 000 trajectories dissociating within 500 ps.
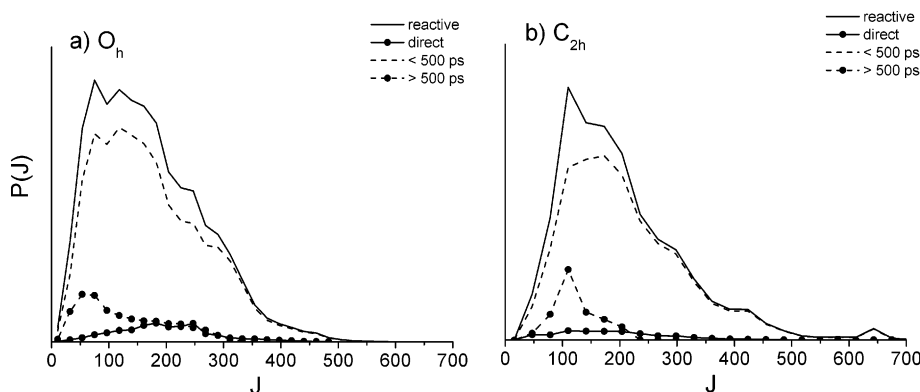
Ar-cluster relative energy is transferred to the rotational degrees of freedom.

Opacity functions, i.e., dissociation probabilities as a function of impact parameter, are plotted in Figure 3 for "direct" cluster dissociation. The opacity functions peak at 1.7 and 2.9 Å for the O_h and C_{2h} clusters, respectively, which correspond to a distance slightly less than the distance between the cluster center of mass and the most outerlying atoms of the cluster, i.e., 2 and 3.5 Å, respectively. Hence, these events correspond mainly to collisions of the Ar atom with an outerlying Al atom, far from the cluster center of mass, which is ejected from the cluster upon collision.

For the SID process, the initial vibrational energy and angular momentum distributions are plotted in Figures 4 and 5, respectively. The average excess vibrational energies acquired upon impact are 52.2 and 45.2 kcal mol^{-1} for the O_h and C_{2h} conformers, respectively. These energies are larger and the distributions narrower than in the case of CID. For SID, the average energy transferred to vibration upon collision is almost identical with respect to the Al$_6$ ground-state minimum configuration, but unlike for CID, the distributions of energy are very similar for both conformers. We note that, because of the higher excitation energy, the proportion of dimer and trimer product formation is more significant for SID than for CID (cf. Table 2). Rotational excitations are similar for both conformers and much less significant than in the case of CID, with average angular momentum quantum numbers of 170 and 200 for O_h and C_{2h} clusters, respectively. Finally, for SID, the fraction of clusters dissociating via "direct" dissociation is much lower than that for CID.
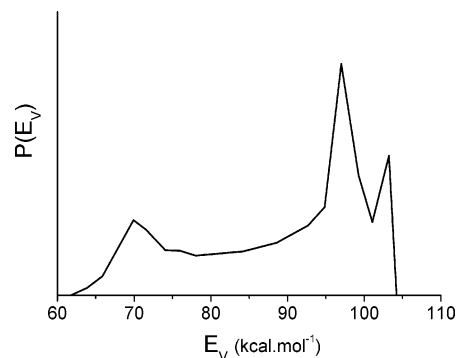
Figure 6. CID vibrational energy distributions for reactive trajectories upon normal collision, i.e., zero impact parameter for the O_h cluster.

These features are all consistent with the intuitive picture where collision with a surface excites many vibrational modes at once and is unlikely to result in direct ejection of an outerlying atom of the cluster, at least for normal collisions. For SID, the initial cluster conformer shape only slightly affects how the excitation energy is distributed among the various degrees of freedom upon collision (cf. Figures 3 and 4), whereas this effect is more pronounced in the case of CID (cf. Figures 1 and 2). Therefore, the excitation mechanism appears to have a strong influence on the way the excitation energy is distributed among the vibrational and rotational degrees of freedom. The differences observed in the excitation energy distributions for CID and SID are mainly due to the different impact parameter distributions involved in both processes. As an illustration, the CID vibrational energy distribution at zero impact parameter,
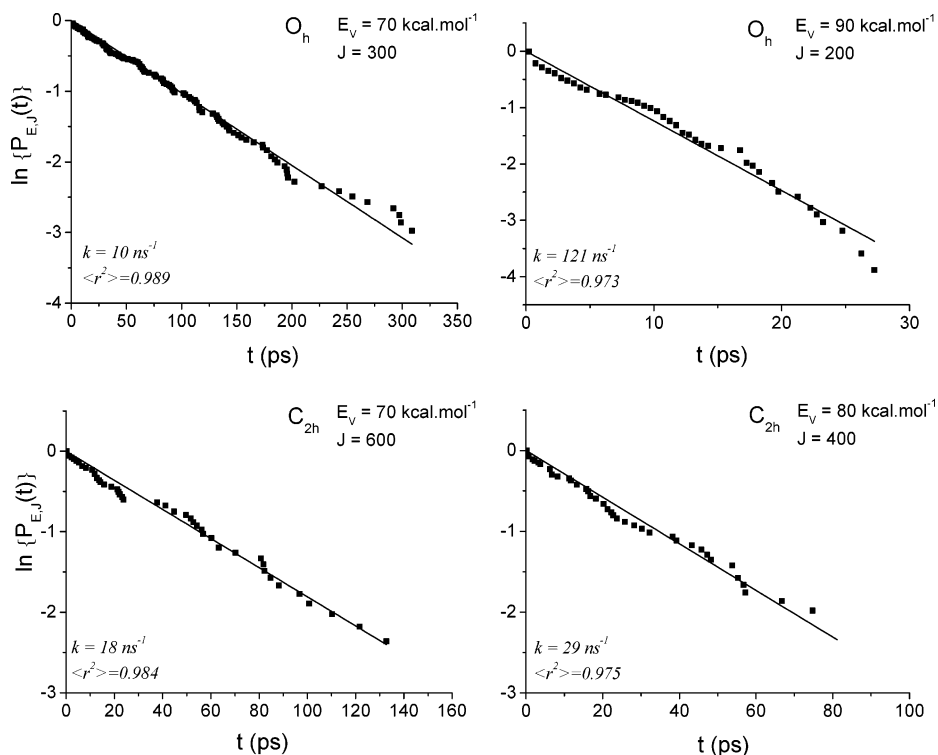
Figure 7. Logarithmic plot of the Al_6 excited cluster normalized population as a function of time for the CID of O_h (upper panels) and C_{2h} (lower panels) clusters at selected E_V and J values. Dots represent the results of simulations and the solid line the fit to eq 4 yielding the microcanonical rate constant indicated on each plot. The correlation coefficient resulting from the fit $\langle r^2 \rangle$ is also given.

Figure 8. Logarithmic plot of the Al_6 excited cluster normalized population as a function of time for the SID of O_h (upper panels) and C_{2h} (lower panels) clusters at selected E_V and J values. Dots represent the results of simulation and the solid line the fit to eq 4 yielding the microcanonical rate constant indicated on each plot. The correlation coefficient resulting from the fit $\langle r^2 \rangle$ is also given.
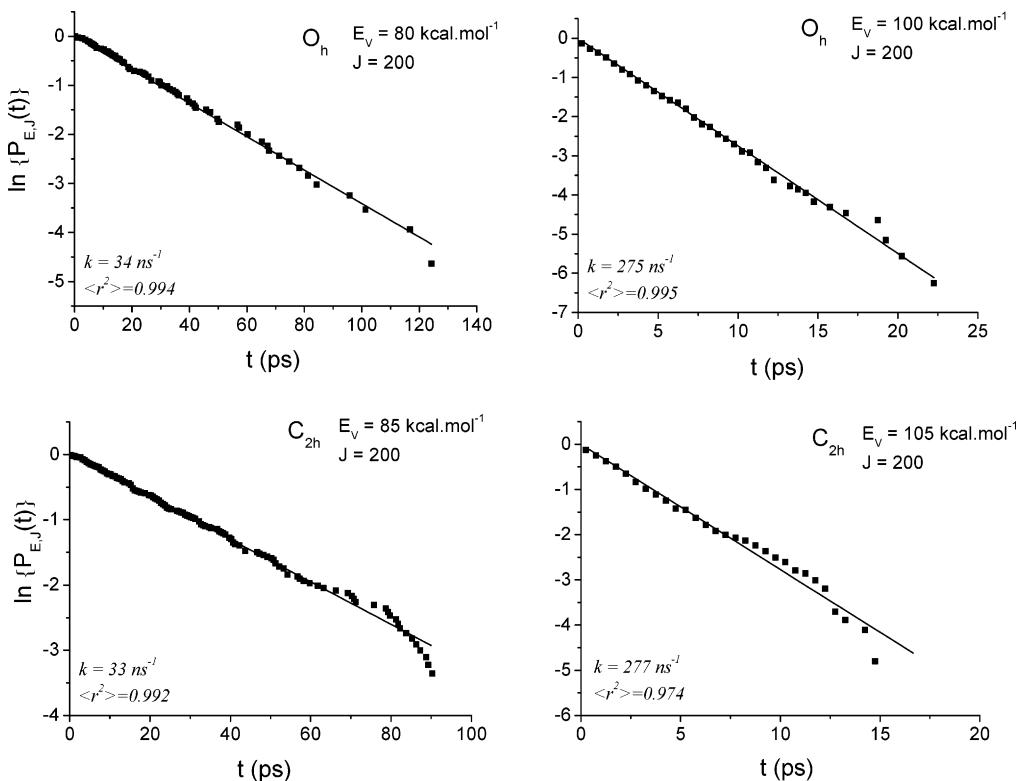
i.e., for normal collisions, which is shown in Figure 6 for the O_h cluster, is very similar to its SID counterpart (Figure 4). Nevertheless, even for non-normal collisions, the SID rotational state distribution of excited clusters is expected to be much colder than in CID because of the hindrance of the whole cluster rotational motion by the surface.

B. Cluster Lifetimes and (E, J) Resolved Unimolecular Rate Constants. The population of excited clusters with a given

TABLE 4: Simulated and OTS/PST Rate Constants[a]

$E_v{}^b$	$E_r{}^c$	J	k_{simul} CID	SID	$k_{OTS/PST}$
O_h ($E_0 = 38.8$ kcal mol^{-1})					
60	1.1	100	0.4		0.6
	4.4	200	0.6		1.4
	9.9	300	1.4		5
	17.6	400	3		29
70	1.1	100	8	8	9
	4.4	200	8	6	17
	9.9	300	11	10	46
	17.6	400	16		149
	27.5	500	22		305
80	1.1	100	43	30	66
	4.4	200	41	34	97
	9.9	300	56	48	175
	17.6	400	63	58	353
90	1.1	100	91	115	184
	4.4	200	121	117	232
	9.9	300		134	342
	17.6	400		185	594
100	1.1	100	221	231	320
	4.4	200		275	393
	9.9	300		271	569
110	1.1	100	401		553
	4.4	200	466		675
C_{2h} ($E_0 = 43.8$ kcal mol^{-1})					
70	9.9	300	6		17
	17.6	400	6		74
	27.5	500	11		3
	39.6	600	18		100
75	1.1	100		7	9
	4.4	200		8	17
80	9.9	300	24		101
	17.6	400	29		248
	27.5	500	39		605
85	1.1	100		32	66
	4.4	200		33	97
95	1.1	100		133	184
	4.4	200		120	232
	9.9	300		147	342
105	1.1	100		244	320
	4.4	200		277	393
	9.9	300		282	569
115	1.1	100		429	553
	4.4	200		442	675

[a] Energies in kcal mol^{-1} and rate constants in ns^{-1}. [b] With respect to the minimum structure energy. [c] Rotational energy.

vibrational energy E_V and total angular momentum J (or equivalently total energy E and J), was monitored as a function of time for both conformers and both excitation processes. In all cases, the simulated cluster population was found to decrease exponentially, and unimolecular rate constants were evaluated by fitting the normalized cluster population decay with eq 4. As the distribution of internal energy acquired upon collision cannot be controlled in simulations, a very large number of trajectories was necessary to obtain (E, J) resolved cluster populations and rate constants over a wide range of excitation energies and angular momenta, i.e., 40 000 trajectories dissociating within 500 ps for each process and conformer were necessary to obtain converged results. Obviously, the range of excitation energies and angular momenta is imposed by the partitioning of energy resulting from the excitation mechanism (cf. Figures 1 and 2 and Figures 4 and 5). Figures 7 and 8 display typical (E, J) resolved excited cluster population decays, from which microcanonical rate constants are evaluated. Comparison is made between simulated (E, J) rate constants and the predictions of OTS/PST in Table 4 for both O_h and C_{2h} clusters. The simulated unimolecular rate constants are found to be in good agreement with the OTS/PST predictions, as long as the

rotational energy is not too large with respect to the total energy. Indeed, the only discrepancies are found for low vibrational and high rotational excitation energies ($J > 200$ for CID, cf. Table 4). This is most likely due to our approximate treatment of rotational energy levels in the statistical model.[55] Nevertheless, the overall agreement between the simulation results and the predictions of the statistical model is very satisfactory.

The exponential decay of the excited cluster population lifetime distribution shows that, for both CID and SID, the dissociation mechanism is intrinsically RRKM.[14] This suggests that there is no bottleneck for energy redistribution among the vibrational modes in the reactant phase space so that, in a very short time after collision compared to the average time for dissociation, the distribution of the reactant phase space states is microcanonical. Regardless of the excitation mechanism, IVR can be considered instantaneous in both CID and SID, validating the use of statistical models to interpret experimental results.

IV. Summary and Concluding Remarks

The present work aimed at exploring the dynamics of aluminum cluster collision-induced dissociation (CID) and surface-induced dissociation (SID). The main motivation was to investigate, by theoretical methods and simulations, whether the generally accepted assumption of a statistical behavior was valid for such processes. The dynamics of Al$_6$ dissociation was followed in time by classical trajectory simulations after collision with either an Ar atom or a model surface. The initial vibrational energy and angular momentum distributions resulting from collision, as well as the energy and angular momentum resolved lifetime distributions, of excited clusters were determined for both processes.

The partitioning of excitation energy acquired upon collision was found to depend on the excitation mechanism (CID or SID), as well as on the cluster molecular shape, especially in the case of CID, but shared similar features. For both types of processes, the energy and angular momentum resolved excited cluster lifetime distributions were found to decay exponentially, in agreement with statistical theories of chemical reactions, suggesting intrinsic RRKM behavior. Moreover, the simulated microcanonical rate constants determined from the lifetime distribution decay are in good agreement with the predictions of the OTS/PST model, which further proves the statistical character of the cluster CID and SID. We thus conclude that, for the Al$_6$ cluster CID and SID considered here, the rate of IVR is much faster than the dissociation rate, whatever the excitation mechanism.

However, though it appears valid to treat the dissociation step as a statistical process, the models used to determine cluster binding energies from experimental CID/SID cross sections employ approximate internal energy distributions resulting from collision. For instance, as mentioned in the Appendix of ref 69, the energy transferred to clusters in CID experiments is estimated through an empirically modified version of the line-of-center (LOC) model,[70] which allows an analytical derivation of the CID cross section. This model implicitly assumes a spherical shape for the cluster. As shown in this work, the cluster shape might significantly influence the collision-induced distribution of internal energy, and accordingly, the development of simple models that accurately predict energy transfer upon collision appears of prime importance.

References and Notes

(1) Bernstein, R. *Chemical Reactions in Clusters*; Oxford University Press: New York, 1996.

(2) Haberland, H. *Clusters of Atoms and Molecules I*; Springer: Berlin, 1994.

(3) Kawazoe, Y.; Kondow, T.; Ohno, K. *Clusters and Nanomaterials*; Theory and Experiments; Springer: Berlin, 2002.

(4) Castleman, A. W.; Bowen, K. H. *J. Phys. Chem.* **1996**, *100*, 12911.

(5) Bacic, Z.; Miller, R. E. *J. Phys. Chem.* **1996**, *100*, 12945.

(6) Armentrout, P. B. *Annu. Rev. Phys. Chem.* **2001**, *52*, 423.

(7) Truhlar, D. G.; Garrett, B. C.; Klippenstein, S. J. *J. Phys. Chem.* **1996**, *100*, 12771.

(8) Forst, W. *Theory of Unimolecular Reactions*; Academic: New York, 1973.

(9) Pechukas, P. *Annu. Rev. Phys. Chem.* **1981**, *32*, 159.

(10) Pollack, E. *Theory of Chemical Reaction Dynamics*; GRC: Boca Raton, FL, 1985.

(11) Steinfeld, J. I.; Fransisco, J. S.; Hase W. L. *Chemical Kinetics and Dynamics*; Prentice Hall. Inc.: Upper Saddle River, NJ, 1989.

(12) Gilbert, R. G.; Smith, S. C. *Theory of Unimolecular and Recombination Reactions*; Blackwell: Oxford, U.K., 1990.

(13) Holbrook, K. A.; Pilling, M. J.; Robertson, S. H. *Unimolecular Reactions*; Wiley: New York, 1996.

(14) Baer, T.; Hase, W. L. *Unimolecular Reaction Dynamics*; Oxford University Press: Oxford, NY, 1996.

(15) Leitner, D. M.; Levine, B.; Quenneville, J.; Martinez, T. J.; Wolynes, P. G. *J. Phys. Chem A* **2003**, *107*, 10706.

(16) Leitner, D. M.; Wolynes, P. G. *J. Phys. Chem A* **1997**, *101*, 541.

(17) Baer, T.; Potts, A. R. *J. Phys. Chem. A.* **2000**, *104*, 9397.

(18) Keske, J. C.; Pate, B. H. *Annu. Rev. Phys. Chem.* **2000**, *51*, 323.

(19) Roncero, O.; Halberstadt, N.; Beswick, J. A. *Adv. Multi-Photon Processes Spectrosc.* **1998**, *11*, 99.

(20) Nesbitt, J. D. *Jerusalem Symp. Quantum Chem. Biochem.* **1991**, *24*, 113.

(21) King, S. D. *NATO ASI Ser.* **1987**, *Ser. C 212,* 593.

(22) Vainhaus, S. B.;. Gislason, E. A.; Hanley, L. *J. Am. Chem. Soc.* **1997**, *119*, 4001 and reference therein.

(23) Rodgers, M. T.; Ervin, K. M.; Armentrout, P. B. *J. Chem. Phys.* **1997**, *106*, 4499.

(24) Rodgers, M. T.; Armentrout, P. B. *J. Chem. Phys.* **1998**, *109*, 1787.

(25) Spasov, V. A.; Ervin, K. M. *J. Chem. Phys.* **1998**, *109*, 5344.

(26) Ray, U.; Jarrold, M. F.; Bower, J. E.; Kraus, J. S. *J. Chem. Phys.* **1989**, *91*, 2912.

(27) Jarrold, M. F.; Creegan, M. K. *Int. J. Mass Spectrom. Ion Processes* **1990**, *102*, 161.

(28) Engelking, P. C. *J. Chem. Phys.* **1986**, *85*, 3103.

(29) Engelking, P. C. *J. Chem. Phys.* **1987**, *87*, 937.

(30) Klots, C. E. *J. Phys. Chem.* **1988**, *92*, 5864.

(31) Klots, C. E. *J. Chem. Phys.* **1989**, *90*, 4470.

(32) Klots, C. E. *J. Phys. Chem.* **1992**, *96*, 1733.

(33) Howard, J. A.; Sutcliffe, R.; Tse, J. S.; Dahmane, H.; Mile, B. *J. Phys. Chem.* **1985**, *89*, 3595.

(34) Cox, D. M.; Trevor, D. J.; Whetten, R. L.; Rohlfing, E. A.; Kaldor, A. *J. Chem. Phys.* **1986**, *84*, 4651.

(35) Cox, D. M.; Trevor, D. J.;. Whetten, R. L.; Kaldor, A. *J. Phys. Chem.* **1988***, 92*, 421.

(36) Schriver, K. E.; Persson, J. L.; Honea, E. C.; Whetten, R. L. *Phys. Rev. Lett.* **1990**, *64*, 2539.

(37) Begemann, W.; Meiwes-Broer, K. H.; Lutz, H. O. *Phys. Rev. Lett.* **1986**, *56*, 2248.

(38) Ray, U.; Jarrold, M. F.; Bower, J. E.; Kraus, J. S. *Chem. Phys. Lett.* **1989**, *159*, 221.

(39) Saunders: W. A.; Fayet, P.; Woste, L. *Phys. Rev. A* **1989**, *39*, 4400.

(40) Cottancin, E.; Pellarin, M.; Lerme, J.; Baguenard, B.; Palpant, B.; Vialle, J. L.; Broyer, M. *J. Chem. Phys.* **1997**, *107*, 757.

(41) Jarrold, M. F.; Bower, J. E.; Kraus, J. S. *J. Chem. Phys.* **1987**, *86*, 3876.

(42) Jarrold, M. F.; Bower, J. E. *J. Chem. Phys.* **1987**, *87*, 5728.

(43) Hanley, L.; Ruatta, S. A.; Anderson, S. L. *J. Chem. Phys.* **1987**, *87*, 260.

(44) Begemann, W.; Hector, R.; Liu, Y. Y.; Tiggesbaumker, J.; Meiwes-Broer, K. H.; Lutz, H. O. *Z. Phys. D* **1989**, *12*, 229.

(45) Kaya, K.; Fuke, K.; Nonose, S.; Kikuchi, N. *Z. Phys. D* **1989,** *12*, 571.

(46) Ruatta, S. A.; Anderson, S. L. *J. Chem. Phys.* **1988**, *89*, 273.

(47) Ingolfsson, O.; Busolt, U.; Sugawara, K. J. *J. Chem. Phys* **1999**, *110*, 4382.

(48) Basch, H. *Chem. Phys. Lett.* **1987**, *136*, 289.

(49) Upton, T. H. *Phys. Rev. Lett.* **1986,** *56*, 2168; *J. Chem. Phys.* **1987**, *86*, 7054; *J. Phys. Chem.* **1986**, *90*, 754.

(50) Pacchioni, G.; Koutecky, J. *Ber. Bunsen-Ges. Phys. Chem.* **1984**, *88*, 242.

(51) Meier, U.; Peyerimhoff, S. D.; Grein, F. *Z. Phys. D* **1990**, *17*, 209.

(52) Jug, K.; Schluff, H. P.; Kupka, H.; Iffert, R. J. *Comput. Chem.* **1988**, *9*, 803.

(53) Jones, R. O. *Phys. Rev. Lett.* **1991,** *67,* 224; *J. Chem. Phys.* **1993**, *99*, 1194.

(54) Petterson, L. G. M.; Bauschlicher, C. W.; Halicioglu, T. *J. Chem. Phys.* **1987**, *87*, 2205.

(55) Peslherbe, G. H.; Hase, W. L. *J. Chem. Phys.* **1996**, *105*, 7432.

(56) Peslherbe, G. H.; Hase, W. L. *J. Chem. Phys.* **1996**, *104,* 9445.

(57) Peslherbe, G. H.; Hase, W. L. *J. Chem. Phys.* **1994**, *101*, 8535.

(58) de Sainte Claire, P.; Peslherbe, G. H.; Hase, W. L. *J. Phys. Chem.* **1995**, *99*, 8147; de Sainte Claire, P.; Hase, W. L. *J. Phys. Chem.* **1996**, *100*, 8190.

(59) Peslherbe, G. H.; Hase, W. L. *J. Phys. Chem. A* **2000**, *104*, 10556.

(60) Light, J. C. *Discuss. Faraday Soc.* **1967**, *44*, 14.

(61) Pachukas, P.; Light J. C. *J. Chem. Phys* **1965**, *42,* 3281.

(62) Nikitin, E. *Theor. Exp. Chem.* **1965**, *1*, 83.

(63) Chesnavich, W. J.; Bowers, M. T. *Gas-Phase Ion Chemistry*; Bowers, M. T., Ed.; Academic: New York, 1979.

(64) *Venus*, Hase, W. L.; Duchovic, R. J.; Hu, X.; Komornicki, A.; Lim, K. F.; Lu, D. H.; Peslherbe, G. H.; Swamy, K. N.; Vande Linde, S. R.; Varandas, A.; Wang, H.; Wolf, R. J. *QCPE* **1996**, *16*, 671.

(65) Axilrod, B. M.; Teller, E. J. *Chem. Phys.* **1943**, *11*, 299.

(66) Rao, B.; Jena, P. J. *J. Chem. Phys.* **1999**, *111*, 1890.

(67) Vach, H. *Phys. Rev. B* **2000**, *61*, 2310.

(68) Peslherbe, G. H.; Hase, W. L. *Theory of Atomic and Molecular Cluster*; Jellinek, J., Ed.; Springer: New York, 1999.

(69) Khan, F. A.; Clemmer, D. E.; Schultz, R. H.; Armentrout, P. B. *J. Phys. Chem.* **1993**, *97*, 7978.

(70) Levine, R. D.; Bernstein, R. B. *Molecular Reaction Dynamics and Chemical Reactivity*; Oxford University Press: New York, 1987; pp 59–60.